The Artificial Leaf

DANIEL G. NOCERA*

Department of Chemistry, 6-335, Massachusetts Institute of Technology, 77 Massachusetts Avenue, Cambridge, Massachusetts 02139-4307, United States

RECEIVED ON NOVEMBER 23, 2011

CONSPECTUS

To convert the energy of sunlight into chemical energy, the leaf splits water via the photosynthetic process to produce molecular oxygen and hydrogen, which is in a form of separated protons and electrons. The primary steps of natural photosynthesis involve the absorption of sunlight and its conversion into spatially separated electron—hole pairs. The holes of this wireless current are captured by the oxygen evolving complex (OEC) of photosystem II (PSII) to oxidize water to oxygen. The electrons and protons produced as a byproduct of the OEC reaction are captured by ferrodoxin of photosystem I. With the aid of ferrodoxin—NADP$^+$ reductase, they are used to produce hydrogen in the form of NADPH. For a synthetic material to realize the solar energy conversion function of the leaf, the light-absorbing material must capture a solar photon to generate a wireless current that is harnessed by catalysts, which drive the four electron/hole fuel-forming water-splitting reaction under benign conditions and under 1 sun (100 mW/cm^2) illumination.

This Account describes the construction of an artificial leaf comprising earth-abundant elements by interfacing a triple junction, amorphous silicon photovoltaic with hydrogen- and oxygen-evolving catalysts made from a ternary alloy (NiMoZn) and a cobalt—phosphate cluster (Co-OEC), respectively. The latter captures the structural and functional attributes of the PSII-OEC. Similar to the PSII-OEC, the Co-OEC self-assembles upon oxidation of an earth-abundant metal ion from 2+ to 3+, may operate in natural water at room temperature, and is self-healing. The Co-OEC also activates H$_2$O by a proton-coupled electron transfer mechanism in which the Co-OEC is increased by four hole equivalents akin to the S-state pumping of the Kok cycle of PSII. X-ray absorption spectroscopy studies have established that the Co-OEC is a structural relative of Mn$_3$CaO$_4$—Mn cubane of the PSII-OEC, where Co replaces Mn and the cubane is extended in a corner-sharing, head-to-tail dimer.

The ability to perform the oxygen-evolving reaction in water at neutral or near-neutral conditions has several consequences for the construction of the artificial leaf. The NiMoZn alloy may be used in place of Pt to generate hydrogen. To stabilize silicon in water, its surface is coated with a conducting metal oxide onto which the Co-OEC may be deposited. The net result is that immersing a triple-junction Si wafer coated with NiMoZn and Co-OEC in water and holding it up to sunlight can effect direct solar energy conversion via water splitting. By constructing a simple, stand-alone device composed of earth-abundant materials, the artificial leaf provides a means for an inexpensive and highly distributed solar-to-fuels system that employs low-cost systems engineering and manufacturing. Through this type of system, solar energy can become a viable energy supply to those in the non-legacy world.

In his 1912 paper in *Science*,[1] Giacomo Ciamician posed a compelling challenge—*to fix the solar energy through suitable photochemical reactions with new compounds that master the photochemical processes that hitherto have been the guarded secret of the plants*. The most important of these photochemical processes is the splitting of water to oxygen and hydrogen. Photosynthesis produces the energy that sustains life on our planet by using solar light to rearrange the bonds of water to oxygen and hydrogen; the hydrogen is fixed by its combination with carbon dioxide to produce carbohydrate (Figure 1).[2] Analysis of the energetics of the solar fuels conversion process shows that it is water splitting and not carbohydrate production that is at the heart of solar energy storage. The reversible potential for the water splitting reaction is
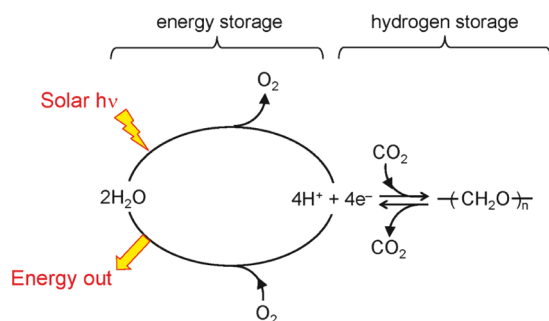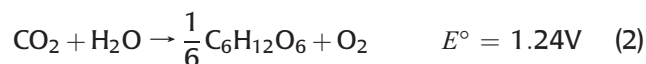
$$H_2O \rightarrow H_2 + \frac{1}{2}O_2 \qquad E^\circ = 1.23V \qquad (1)$$

FIGURE 1. The solar photons are stored by photosynthesis to split water to oxygen and four protons and four electrons, which are utilized in the conversion of carbon dioxide to carbohydrates. Adapted from Barber, ref 2.

whereas the reversible potential for production of carbohydrate from water and CO_2 is

$$CO_2 + H_2O \rightarrow \frac{1}{6} C_6H_{12}O_6 + O_2 \qquad E^\circ = 1.24V \quad (2)$$

Note that water splitting is subsumed by reaction 2. As illustrated by the thermodynamic potentials for reactions 1 and 2, on an electron equivalency basis, the production of the carbohydrate stores only 0.01 eV more energy than water splitting. Thus, solar energy storage in photosynthesis is achieved by water splitting; carbohydrate production is nature's method of storing the hydrogen that is released from the water splitting reaction. Consequently, the key to duplicating photosynthesis lies squarely in the ability to achieve solar-driven water splitting by a direct method.

This Account describes a discovery that meets Ciamician's challenge from a century ago: (1) the creation of oxygen- and hydrogen-evolving compounds that master water splitting under the conditions and with the properties of the natural photosynthetic reaction and (2) the integration of these compounds with a light-harvesting semiconductor to create an artificial leaf. The achievement of the objectives of 1 and 2 permits direct solar-to-fuels conversion to be achieved under 1 sun (AM 1.5, 100 mW/cm^2) illumination.

Photosynthesis and Water Splitting

The compound that achieves water splitting in photosynthesis is the oxygen evolving complex (OEC), which resides in photosystem II (PSII). The OEC is "charged" by a solar-driven wireless current as shown in Figure 2. Light absorption in the reaction center of PSII produces an electronically excited electron. The hole (×4) produced from electron transfer is passed within PSII to the OEC, which performs the critical
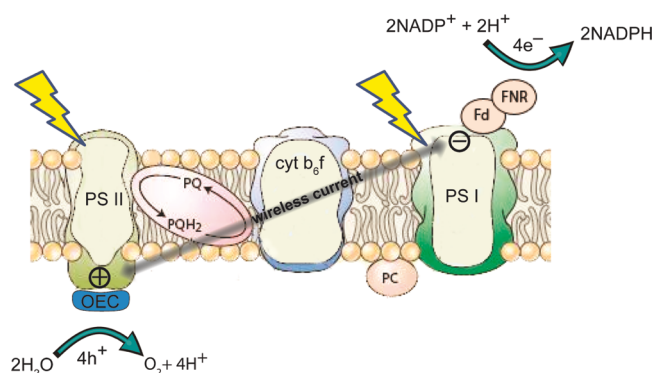

FIGURE 2. A simplified scheme of the light-driven reactions of photosynthesis. Solar photons create a wireless current that is harnessed by redox cofactors at the terminus of the charge-separating network to translate the wireless current into a solar fuel by performing the water splitting reaction at OEC. The initial reductant, plastoquinol (PQH_2), is translated into NADPH in PSI, which transfers "hydrogen" to the Calvin cycle where it is fixed with CO_2 to produce carbohydrates.

water-splitting step to release O_2 and four protons. The electrons are transferred via a series of redox-active cofactors to photosystem I (PSI). These cofactors include plastoquinol (PQH_2) and plastocyanin (PC) and those bound within the cytochrome b_6f (cyt b_6f) complex finally arriving at ferredoxin (Fd) bound to PSI (see Figure 2). Through the action of ferredoxin–$NADP^+$ reductase (FNR), these energized electrons reduce protons to produce hydrogen in the form of NADPH.[3] In executing this reaction sequence, the plant stores solar energy in a fuel-forming process resulting from rearranging the bonds of water.

A key design element of photosynthesis is the separation of the functions of light collection and conversion from that of catalysis. This separation is dictated by the thermodynamics of the water-splitting reaction. To match the solar spectrum and at the same time deliver oxidizing and reducing equivalents of sufficient potential to split water and reduce $NADP^+$, PSII and PSI are confined to generating an electron/hole pair one photon at a time. However, water splitting is a four-electron/hole process,[4] while $NADP^+$ reduction is a two-electron/proton reaction. Hence, the placement of the multielectron catalysts at the termini of the charge-separating network is compulsory so that the one photon–one electron/hole equivalency of the solar-driven wireless current can be bridged to the four-electron/hole chemistry of water splitting.

Many of the "guarded secrets" of the photosynthetic solar fuels process of Figure 2 have been revealed by science over the past decade. Most important of these secrets is the structure of the PSII-OEC. The X-ray crystal structure of the membrane-bound PSII has been solved at increasing resolution to reveal the composition and atomic organization of
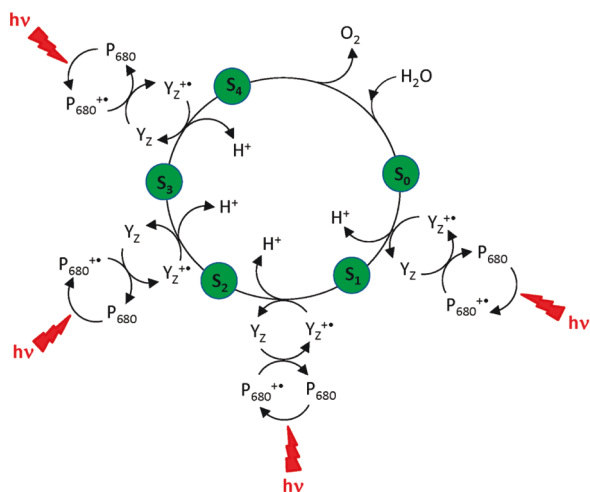
FIGURE 3. The S-state (Kok) cycle showing how the absorption of four photons of light ($h\nu$) by P680 drives the splitting of two water molecules and formation of O_2 through a consecutive series of five intermediates (S0, S1, S2, S3, and S4). The S-states represent the various oxidation states of Mn in PSII-OEC. Electron donation from the PSII-OEC to P680[•+] is mediated by tyrosine, Y_Z. Adapted from Barber, ref 2.

the OEC and the details of its protein environment.[5,6] The OEC comprises a cube of three manganese atoms and one Ca ion; a fourth manganese atom hangs from the cube via bridging oxygens. It is this simple Mn_4Ca cluster that collects the four hole equivalents produced by solar irradiation of PSII and accomplishes water splitting. To do so, four design elements involving the OEC have been implemented by the photosynthetic machinery.

Cluster Self-Assembly. The Mn_4Ca cluster self-assembles by an oxidative mechanism[7] involving the photo-oxidation of Mn^{2+} ions to Mn^{3+} ions bound to the apo-coordination environment[8] of the PSII complex. The oxidizing equivalents are passed via the same P680–Y_Z pathway that is used for water splitting after the OEC is assembled.

Proton-Coupled Electron Transfer (PCET) Catalysis. The single electron and single hole flow are sequentially advanced to four electron/hole equivalency by photon absorption according to the S-state Kok cycle shown in Figure 3. The progression through the S-states results in the storage of four oxidizing equivalents in the OEC by raising the oxidation state of the Mn ions to a sufficiently high potential to enable water splitting.[9] We have shown in model studies that the critical O–O bond forming step should occur by coupling the release of a proton to the third hole equivalent of the Kok cycle.[10,11]

Catalyst Repair. The water splitting reaction produces reactive oxygen species that are toxic to the organism. To counteract the degrading effects of light, photosynthetic organisms undergo constant repair by using proteases[12] to remove oxidatively photodamaged constituents of PSII.[13,14] The D1 protein, which provides most of the ligands in the protein environment to OEC, is a particular target of this repair cycle. Upon its removal, the OEC disassembles. The proteolytic degradation of the photodamaged D1 is accompanied by cotranslational insertion of newly synthesized D1 into the membrane as frequently as every 30 min for some organisms.[13,15] Upon re-insertion of D1, the OEC reassembles. Thus photosynthesis invests its efforts in continually repairing an unstable catalyst rather than preparing a stable catalyst.

Operation in Environmental Conditions. The OEC operates from natural water sources, at ambient conditions of temperature and pressure, and at neutral and near-neutral pHs and uses earth-abundant elements. These conditions are precisely opposite to the conditions used by present water-splitting technologies, which perform water splitting in highly engineered and harsh environments or with rare elements or both.[16]

An Artificial OEC

Using the foregoing design principles of photosynthesis as a roadmap, we have created artificial OEC catalysts comprising Co and phosphate (P_i)[17] or Ni and borate (B_i).[18] The catalysts *self-assemble* from aqueous solution, and they are *structural analogs* to that of PSII-OEC. Water splitting is accomplished by *PCET* where P_i (or B_i) anion manages the coupling of the proton to the electron released from water oxidation; the anion also provides a mechanism for *repair*. The catalysts are extremely versatile and *operate under environmental conditions*. Details of the artificial OEC are presented below for the CoP$_i$ (B_i) system, which is designated as Co-OEC; the Ni–B_i catalyst possesses properties akin to CoP$_i$, and they will not be discussed here.

Self-Assembly of a Cubane Cluster That Is a Structural Analog to PSII-OEC. An artificial OEC composed of cobalt, oxygen, and phosphate self-assembles upon the oxidation of Co^{2+} to Co^{3+} ion in aqueous solution.[17,19] Alternatively, the Co-OEC may be grown from cobalt metal films under anodization conditions.[20] As shown in Figure 4, smooth thin films of the catalyst are formed if oxidation is performed at a prepotential to water oxidation (1.1 V vs NHE); rougher films form if the oxidation is performed at a potential where water oxidation also occurs (1.3 V vs NHE). All films, whether smooth or roughened, are active catalysts. Dissolved cobalt is not needed for catalyst operation; once formed, the catalyst film may be immersed in a solution of only phosphate and water splitting activity is maintained. The mild
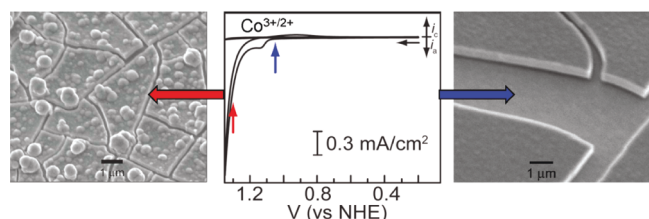
FIGURE 4. Dried catalyst films formed from solutions of Co(aq)$^{2+}$ and P$_i$ under (right) quiescent (0.85 V vs Ag/AgCl) and (left) catalytically active (1.1 V vs Ag/AgCl) conditions on an ITO substrate.
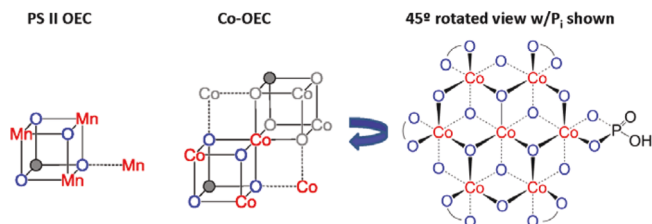

FIGURE 5. (left) Schematic of cubane structure of PSII-OEC. (middle) Structure of the Co-OEC as determined from EXAFS (P$_i$ not shown). Co-OEC is the head-to-tail dimer of the cubane of PSII-OEC. (right) Co-OEC structure rotated by 45° to more clearly shows edge sharing octahedra. The alkali metal ions, which are not shown, likely reside above the 3-fold triangle defined by the μ-bridging oxygens.

aqueous electrodeposition conditions permit conformal catalyst layers to be deposited at a desired thickness on a surface of any architecture. The self-assembly of the Co-OEC may also be photodriven. The Co-OEC self-assembles on the surfaces of irradiated semiconducting materials such as Fe$_2$O$_3$,[21−24] ZnO,[25] or WO$_3$[26] immersed in water containing Co^{2+} and phosphate.

The catalysts films are structurally amorphous and thus X-ray absorption spectroscopy (XAS) was used to structurally characterize Co-OEC. The extended X-ray absorption fine structure (EXAFS) spectra of *in situ* Co-OEC during catalytic turnover[27] and *ex situ* films[28] are consistent with a molecular cobalt complex consisting of edge-sharing CoO$_6$ octahedra. The average size of the molecular cobaltate cluster is seven atoms. The core of Co-OEC is a nearly identical structural congener of the PSII-OEC as schematically illustrated in Figure 5. Both systems are a partial cubane with identical metal−metal (d = 2.82 Å) and metal−oxo (d = 1.89 Å) distances. In OEC, the cube is completed with a Ca^{2+} ion; though the alkali metal ions for CoP$_i$ have not been located, they likely reside on the 3-fold oxygen triangle to complete the cube structure, as is the case for cobaltates.[29] The edge Co atoms of the cluster are likely terminated by the phosphate ions, which have been shown to be exchangeable.[30]

A Highly Active PCET Water-Splitting Catalysis. Co-OEC performs water oxidation at neutral pH. The catalyst

operates at 350 mV lower overpotential than Pt at all current densities and under neutral conditions. Current densities as high as 100 mA/cm^2 (geometric surface area) have been achieved at overpotentials as low as 360 mV (67% energy conversion efficiency).[31] The high current density is maintained for days with no discernible drop in activity. The Faradaic efficiency of the catalyst is 100%; that is, the catalyst is selective for O$_2$ production from water, and no other product is obtained.

As in PSII-OEC, water splitting in Co-OEC occurs from the +4 oxidation state. Co-OEC catalyst films exhibit EPR signals corresponding to populations of both Co(II) and Co(IV).[32] Figure 6 shows the EPR spectrum of Co-OEC under deposition conditions compared with Co(II)-containing species (top panel, left), Co-OEC under an applied voltage at which catalysis occurs (middle panel, left), and a Co$_4$O$_4$ cubane containing cobalt in the +4 oxidation state (bottom panel, left). The presence of Co(IV) is clearly established at potentials where OER catalysis occurs. As the deposition voltage is increased into the region where water oxidation prevails (right panel), the population of Co(IV) rises and the population of Co(II) decreases. The spin distribution of Co(IV) has been examined by EPR for a cobalt−oxo cubane cluster possessing formal cobalt oxidation states III, III, III, and IV.[33] Davies ENDOR, mims ^{1}H ENDOR, and multifrequency ^{14}N ESEEM spectra indicate that the unpaired spin is delocalized almost equally across the cobalt atoms, a finding corroborated by DFT calculations. These results suggest that the charge on the Co-OEC catalyst is also highly delocalized.

Insight into the propagation of the catalytically active "holes" of the Co(IV) state through the catalyst film has been afforded by measuring the Co^{III}/Co^{IV} self-exchange kinetics of the Co$_4$O$_4$ cubane compound, [Co$_4$O$_4$(O$_2$CMe)$_2$(bpy)$_4$](ClO$_4$)$_2$,[34] using NMR line broadening techniques.[35]
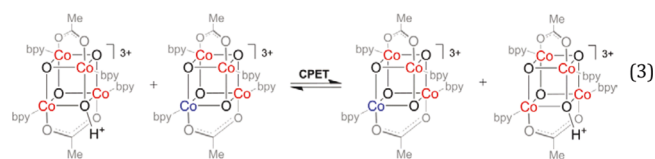
The Co(IV) center is indicated by the blue color coding and Co(III) by red color coding. The second-order rate constant for self-exchange is 1.3 × 10^4 M^{-1} s^{-1} at pH 1. At pH 4, where the cluster is deprotonated, the rate constant increases by a factor of 10 to 3 × 10^5 M^{-1} s^{-1}, consistent with a simple electron-transfer step. A KIE of 4.3 is suggestive of a unidirectional concerted proton−electron transfer (CPET). We have shown that CPET results in order to avoid the high
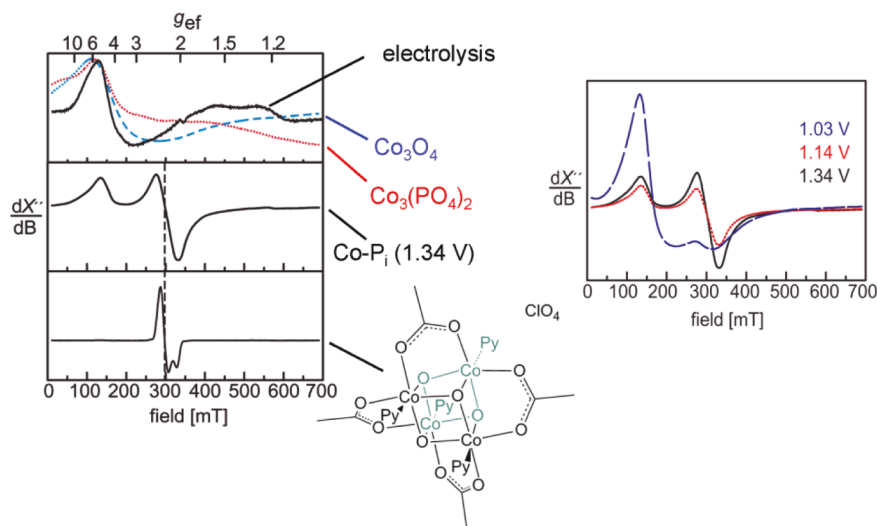
FIGURE 6. CW X-band EPR spectra of (left top) frozen electrolysis solution (—), $Co_3(PO_4)_2$ ($\cdots$), Co_3O_4 ($---$), (left middle) CoP$_i$ catalyst films deposited at 1.34 V, and (left bottom) the Co−oxo cubane $[Co_4O_4(C_5H_5N)_4(CH_3CO_2)_4](ClO_4)$, which exhibits an EPR signal for Co(IV) at $g = 2.27$. (right) Potential dependence of EPR spectrum of catalyst films from 1.03 V, at which catalysis does not occur, to 1.34 V, at which catalysis occurs.
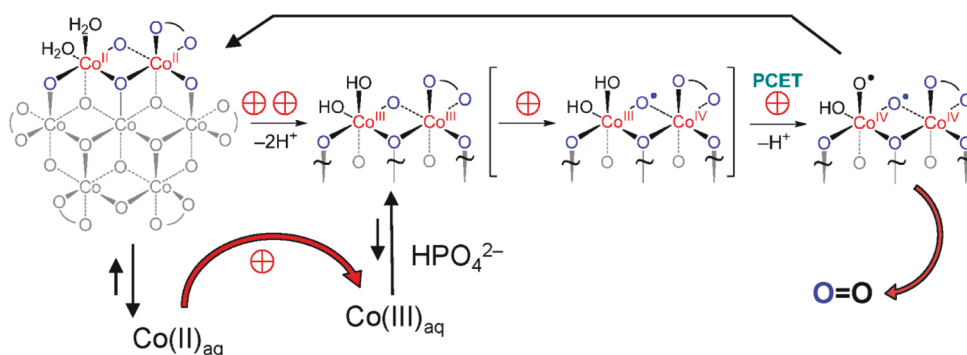

FIGURE 7. Proposed pathway for water splitting by Co-OEC. A PCET equilibrium proceeds the turnover-limiting O−O bond-forming step. Curved lines denote phosphate or terminal oxygen (from water or hydroxide). The oxyl radical in the far right structure is shown for emphasis. If the hole is completely localized on oxygen, then the Co oxidation state is Co(III) and not Co(IV).

energy barrier of >0.16 V imposed by protonation of the Co(IV) species. This result suggests the charge propagation mechanism as hole hopping through catalyst films.

Electrokinetic studies show that the oxidation of Co(III) to Co(IV) is coupled to the loss of a proton.[36] In the absence of phosphate buffer, the overall activity of the Co-OEC is greatly diminished. Together, these studies suggest the PCET mechanism shown in Figure 7. As in PSII-OEC, the redox potential of the Co-OEC is increased by four hole equivalents akin to the S-state pumping of the Kok cycle. The critical step is at the equivalent of the S3 to S4 transition of the Kok cycle. A rapid one-electron, one-proton equilibrium between Co^{III}−OH and Co^{IV}−O in which a phosphate species is the proton acceptor is followed by a chemical turnover-limiting process involving oxygen−oxygen bond coupling. Enriched ^{18}O catalyst operated in unenriched water exhibits extrusion of ^{18}O in

$^{34}O_2$, indicating the participation of a bridging O atom of the catalyst core in the O_2 evolution pathway.[36] Mechanistic details of how the O−O bond forms and the precise nature of the turnover-limiting elementary step remain to be determined.

Water is a poor proton acceptor under neutral conditions. Hence, the activation of oxygen in water requires a bidirectional PCET involving phosphate as a proton acceptor, as has been established in model PCET systems.[37,38] In the Co-OEC mechanism of water splitting, the phosphate plays the essential role of maintaining this PCET equilibrium by facilitating rapid proton transfer with the concomitant oxidation of Co(III) to Co(IV) to furnish the active O_2 producing "S4" state.

A Self-Healing OEC Catalyst. Like PSII-OEC, metal-oxide catalysts are unstable in neutral water and corrode when water splitting is performed under benign conditions. In neutral water, the best base is the metal oxide itself, and
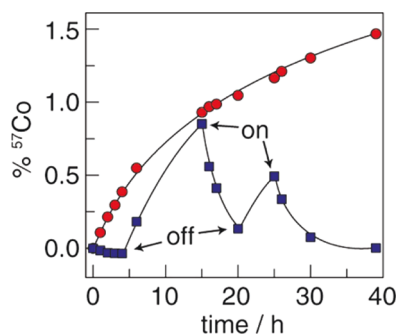
FIGURE 8. Percentage of ^{57}Co leached from films of the CoP$_i$ catalyst on an electrode with a potential bias of 1.3 V (NHE) (■) turned on and off at the times designated and without an applied potential bias (●).

FIGURE 9. Bulk electrolysis profile of anodized Ni (left, 1 M KOH) and CoB$_i$ on ITO (right, 1 M KB$_i$, pH 9.2) anodes in 18 M$\Omega\cdot$cm (———), Charles River water ($\cdots$), and seawater (—). Plots show the overpotential required for electrolysis at 1 mA/cm^2 current density.

consequently the protons produced from water oxidation hasten catalyst corrosion. For the case of Co-OEC, the involvement of the Co(II) oxidation state during catalysis presents an additional challenge to the design of a robust catalyst because Co(II) is high spin and is substitutionally labile. Because the propensity of metal ion dissolution from solid oxides has been shown to correlate with ligand substitution rates,[39] Co-OEC is expected to be structurally unstable in the Co(II) oxidation state. Notwithstanding, the catalytic activity of Co-OEC is maintained owing to its unique ability to undergo self-repair.[30] This repair can be observed directly by monitoring radioactive isotopes of films composed of ^{57}Co (and ^{32}P) during water-splitting catalysis (Figure 8). A dynamic equilibrium is observed for cobalt and phosphate from catalyst films. At open circuit, the appearance of radioactive Co(aq)$^{2+}$ is observed in solution. Upon application of a potential, the cobaltate cluster reforms owing to the equilibrium between Co(aq)$^{3+}$ and phosphate. This result accords well with the original formation of the catalyst films upon oxidation of Co(aq)$^{2+}$ to Co(aq)$^{3+}$. Exchange of phosphate from a terminal ligation site is significantly more facile than the release of a cobalt ion, which is a constituent of a metal−oxo cubane core. The "reversible corrosion" process (shown in Figure 7) engenders the self-healing properties of the Co-OEC, and it permits long-term stability of the Co-OEC. We note that during turnover, the self-exchange rate constant for hole transport is sufficiently large (vide infra) that the film remains in an oxidized state. Thus, self-healing is manifest for reversing catalyst corrosion at open circuit upon reapplication of an anodic potential.

Function in Benign, Environmental Conditions and from Natural Waters. Unlike any known commercial water-splitting catalyst, Co-OEC can operate from a variety of water sources.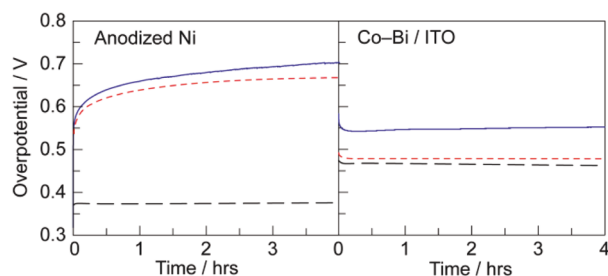 Figure 9 shows the activity of Co-OEC and a commercial anodized Ni oxide catalyst operating in water from the Charles River and in seawater from Woods Hole, MA.[31] For comparative purposes, the operation of Co-OEC and the anodized Ni catalyst in purified water (18 M$\Omega\cdot$cm) is also shown. Whereas stable overpotential values are obtained for the anodized Ni and Co-OEC when operated in purified water, significantly larger overpotential values are required to operate the anodized Ni electrode in Charles River and sea waters, while the overpotential for Co-OEC in these natural waters is little changed. More significantly, the overpotential of the commercial catalyst continues to increase with operation time, indicating that the electrode fouls. At long times, the overall performance of the anodized Ni electrode is significantly reduced. These data suggest the formation of biofilms arising from the denaturation of biomolecules and of passivating oxide layers of indigenous metals commonly found in natural water supplies (e.g., Ca(OH)$_2$, Mg(OH)$_2$), similar to what has been observed previously during the electrolysis of seawater.[40,41] In contrast, the activity of Co-OEC catalyst is stable in waters from the Charles River and from the Atlantic Ocean. The ability of Co-OEC to operate in natural water supplies is likely to be intimately connected to the repair mechanism.

Co-OEC Enables the Use of Simple HER Alloys. Because Co-OEC operates in neutral water, and not harsh conditions, nonprecious metals may be used in place of Pt to produce hydrogen.[42] A NiMoZn cathode for H$_2$ may be electrodeposited from Ni(aq)$^{2+}$ solution, sodium molybdate and anhydrous zinc chloride in the presence of pyrophosphate, bicarbonate, and hydrazine followed by a base leaching solution. Molybdenum leaches from the alloy to furnish high surface area material.[43,44] The alloy achieves current densities of 700 mA/cm^2 at 100 mV overpotential and, with continued leaching, can attain activities as high as at 1000 mA/cm^2 at an overpotential of 35 mV.
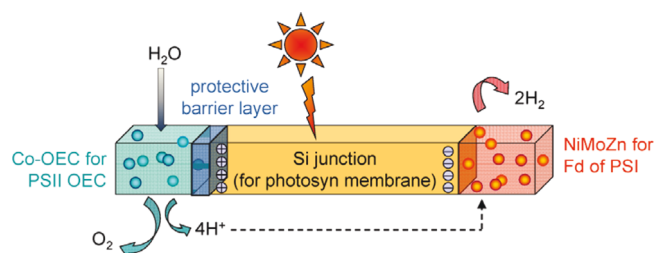
FIGURE 10. Construction of an artificial leaf. The photosynthetic membrane is replaced by a Si junction, which performs the light capture and conversion to a wireless current. The oxygen evolving complex and ferodoxin reductase of the photosynthetic membrane are replaced by Co-OEC and NiMoZn OER and HER catalysts, respectively, to perform water splitting.
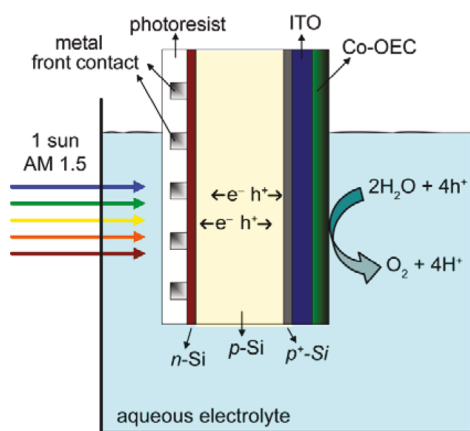

FIGURE 11. Schematic of a Co-OEC functionalized npp^+-silicon single-junction PEC cell. The buried junction performance characteristics are $I_{sc} = 26.7$ mA/cm^2 and $V_{oc} = 0.57$ V.

An Artificial Leaf

The ability to perform water splitting with Co-OEC and NiMoZn catalysts in natural waters, under ambient conditions, and at high and stable current densities provides a direct path to the creation of an artificial leaf, the design elements for which are shown in Figure 10. The function of the photosynthetic membrane to capture solar light and convert it into a wireless current is assumed by Si. The photogenerated single electron and hole are relayed to the Co-OEC and NiMoZn catalysts, until the necessary four electron–hole equivalents are attained to drive the bond rearrangement of water splitting.

Single Junction PEC Cell. The first step to realizing the artificial leaf of Figure 10 is to integrate the Co-OEC with Si. This objective was established by constructing the single junction npp^+ cell shown in Figure 11.[45] The p^+ was incorporated on the p-side of the junction by depositing a 1 μm film of silicon-doped (1%) Al, followed by rapid thermal annealing in N$_2$ at 900 °C.[46] The npp^+-Si single junction
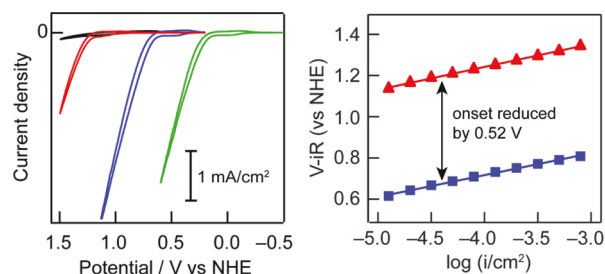

FIGURE 12. (left) CV curves of the single junction npp^+Si|ITO electrode immersed in a 0.1 M KP$_i$ electrolyte in dark (black trace) and that electrode coated with Co-OEC in the dark (red trace), under 1 sun (AM 1.5 illumination, 100 mW/cm^2) (blue trace), and the cell under illumination to which an additional npp^+Si solar cell was connected in series (green trace). The scan rate was 2.5 mV/s for all traces. (right) The npp^+Si|ITO| Co-OEC cell for onset of water oxidation in dark (▲) and at 100 mW/cm^2 illumination (■). Under illumination, the onset potential needed to be applied to the cell is decreased by 0.52 V.

displays improved performance because the space charge region in the p^+ layer is thin enough to act as a tunneling layer. A metal front contact was deposited on the n-side of the sample to enable PEC measurements and was protected from the solution using a 10 μm layer of photoresist. The Si was protected from oxidation by sputtering on the p^+-side of the junction a 50 nm film of ITO, which served as an Ohmic contact for hole transport from the buried Si junction. The Co-OEC catalyst may be electrodeposited on the ITO barrier layer; alternatively the Co-OEC film may be also be grown from thin films of Co on a Si surface.[47]

Figure 12 shows the CV curves of npp^+Si|ITO|Co-OEC immersed in a 0.1 M KP$_i$ electrolyte at pH 7. Under these conditions, the thermodynamic potential for water oxidation is 0.82 V relative to the formal normal hydrogen electrode (NHE). When the potential is applied through the ITO thin film in the dark (black trace in Figure 12), current–voltage characteristics are the same as that of Co-OEC on ITO or FTO electrodes. However, when the structure is illuminated from the n-side with 1 sun (100 mW/cm^2) of AM 1.5 light, the potential onset for water oxidation decreases significantly (blue line in Figure 12). The onset of the cell under illumination requires 0.52 V less applied potential to induce water splitting at a given current density. Noting that this single junction cell generates 0.57 V, the majority of the photovoltage generated by the solar cell is utilized to drive the water splitting reaction. When an additional npp^+Si solar cell was connected in series to npp^+Si|ITO|Co-OEC and both cells were subjected to 1 sun illumination, the onset of the external applied potential is reduced by another 0.5 V (green trace in Figure 12). With these results in hand, we reasoned that the addition of a third Si solar cell would
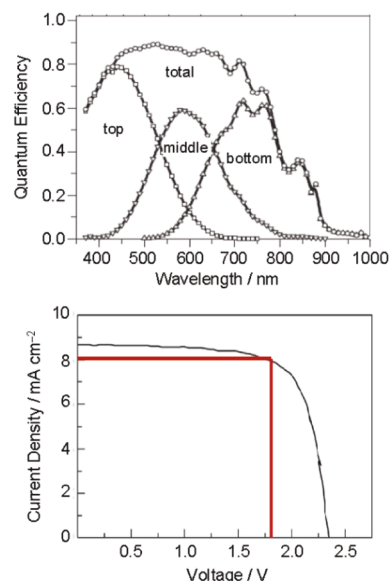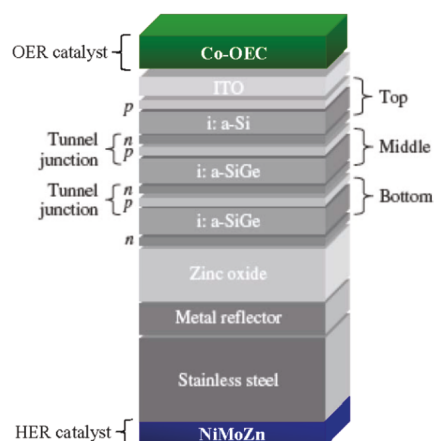
FIGURE 13. The artificial leaf. The *p*-side of 3jn-a-Si solar cell is coated with an ITO protective layer and Co-OEC. The *n*-side is coated with a NiMoZn HER catalyst. The 3jn-a-Si absorption (top right) and current−voltage (bottom right) properties are shown. The overall 3jn-a-Si solar cell efficiency is 6.2%.

provide sufficient potential such that an external potential may be eliminated. Moreover, in seeking to create an artificial leaf, we imposed the further design guidelines of (i) no wiring, (ii) operation of the cell from water under simple conditions, and (iii) performing water splitting under 1 sun illumination.

Triple Junction Wireless Cell: The Artificial Leaf. An artificial leaf comprising earth-abundant materials and that operates under simple conditions and at 1 sun has been realized by interfacing Co-OEC and NiMoZn with a triple junction amorphous Si (3jn-a-Si) solar cell.[42] Stand-alone operation of the cell was achieved with the architecture shown in Figure 13. The 3jn-a-Si produces 8 mA cm^{-2} of current at 1.8 V at an overall efficiency of 6.2%. As in the single junction cell, the *p*-side of the cell was protected with an ITO (or FTO) layer, on which the Co-OEC was electrodeposited. The NiMoZn HER alloy was electrodeposited onto the stainless steel support of the 3jn-a-Si cell. The stainless steel is not needed for the operation of the cell; it is present only as a structural support. The NiMoZn HER alloy may be deposited directly onto Si, and the HER is preserved. When the wireless CoP$_i$|3jn-a-Si|NiMoZn wafer is immersed in an open container of electrolyte (1 M potassium borate, pH 9.2) and illuminated with 1 sun, O$_2$ bubbles evolve from the anode at the front face and bubbles of H$_2$ evolve from the cathode at the back of the wireless cell at an efficiency of 2.5%. Owing to the low solubility of O$_2$ and H$_2$ in water, the solar-to-fuels conversion process may be driven in the absence of a membrane. Overall solar-to-fuels efficiencies

(SFE) were observed to be as high as 4.7% (for a 7.7% solar cell) when Ohmic losses are minimized. Noting that the overall solar-to-fuels efficiency is a product of the overall efficiency for water splitting and solar cell efficiency

$$\text{SFE}(\%) = \varphi(\text{PV}) \cdot \varphi(\text{WS}) \qquad (4)$$

$\varphi(\text{WS})$ is as high as 60%. This value compares well with cell efficiencies based on 3jn-a-Si PVs in which the a-Si is isolated from the electrolyte (SFE = 6% for $\varphi(\text{PV})$ = 10%)[48−50] and for higher-efficiency systems using expensive PV materials (SFE = 18% for $\varphi(\text{PV})$ = 28%).[48−52] Based on $\varphi(\text{WS})$, higher overall cell efficiencies (>10%) may be readily achieved through the use of more efficient PVs. Even further increases in SFE may be realized by implementing engineering designs that minimize Ohmic resistances arising from ion transport.

Conclusions

The artificial leaf achieves direct solar-to-fuels conversion at 1 sun (AM 1.5, 100 mA cm^{-2}) under benign conditions, using earth-abundant materials, and without the use of wires. The artificial leaf mimics nature inasmuch as it stores solar energy in water splitting by conforming to the functional elements of a leaf. We note that the actual leaf does not use hydrogen but stores it as a solid fuel, for example, carbohydrate. In the case of the artificial leaf, the hydrogen is available for combination with CO$_2$ as new catalysts for this process are discovered.

The construction of an artificial leaf is enabled by the Co-OEC. Because water splitting is performed under benign conditions, a simple metal alloy for HER is enabled, and Si may be employed as a stable photovoltaic substrate. The artificial leaf described here, as a simple, stand-alone device composed of earth-abundant materials, provides a first step down a path aligned with the low-cost systems engineering and manufacturing that is required for inexpensive solar-to-fuels systems.[53] In doing so, solar energy can become a viable energy supply to those in the nonlegacy world.[54,55] Considering that it is the 6 billion nonlegacy users that are driving the enormous increase in energy demand by midcentury,[55−57] a research target of delivering solar energy to the poor with discovery such as the artificial leaf provides global society its most direct path to a sustainable energy future.

BIOGRAPHICAL INFORMATION

Daniel G. Nocera is the Henry Dreyfus Professor of Energy at the Massachusetts Institute of Technology. His group studies the basic mechanisms of energy conversion in biology and chemistry with primary focus in recent years on the generation of solar fuels. He has recently exploited catalyst discovery to design an artificial leaf, which duplicates the direct solar fuels process of photosynthesis, the splitting of water to hydrogen and oxygen using light from neutral water, at atmospheric pressure and room temperature, and under 1 sun illumination. This science discovery sets a course for the large scale deployment of solar energy, especially to those of the nonlegacy world.

FOOTNOTES

*E-mail: nocera@mit.edu.
The authors declare no competing financial interest.

REFERENCES

1 Ciamician, G. The Photochemistry of the Future. *Science* **1912**, *36*, 385–394.

2 Barber, J. Photosynthetic Energy Conversion: Natural and Artificial. *Chem. Soc. Rev.* **2009**, *38*, 185–196.

3 Barber, J. Biological Solar Energy. *Philos. Trans. R. Soc., A* **2007**, *365*, 1007–1023.

4 Betley, T. A.; Wu, Q.; Van Voorhis, T.; Nocera, D. G. Electronic Design Criteria for O—O Bond Formation via Metal—Oxo Complexes. *Inorg. Chem.* **2008**, *47*, 1849–1861.

5 Ferreira, K. N.; Iverson, T. M.; Maghlaoui, K.; Barber, J.; Iwata, S. Architecture of the Photosynthetic Oxygen-Evolving Center. *Science* **2004**, *303*, 1831–1838.

6 Umena, Y.; Kawakami, K.; Shen, J.-R.; Kamiya, N. Crystal Structure of Oxygen-Evolving Photosystem II at a Resolution of 1.9 Angstrom. *Nature* **2011**, *473*, 55–65.

7 Burnap, R. L. D1 Protein Processing and Mn Cluster Assembly in Light of the Emerging Photosystem II Structure. *Phys. Chem. Chem. Phys.* **2004**, *6*, 4803–4809.

8 Ananyev, G. M.; Zaltsman, L.; Vasko, C.; Dismukes, G. C. The Inorganic Biochemistry of Photosynthetic Oxygen Evolution/Water Oxidation. *Biochim. Biophys. Acta* **2001**, *1503*, 52–68.

9 Siegbahn, P. E. M. An Energetic Comparison of Different Models for the Oxygen Evolving Complex of Photosystem II. *J. Am. Chem. Soc.* **2009**, *131*, 18238–18239.

10 McGuire, R., Jr.; Dogutan, D. K.; Teets, T. S.; Suntivich, J.; Shao-Horn., Y.; Nocera, D. G. Oxygen Reduction Reactivity of Cobalt(II) Hangman Porphyrins. *Chem. Sci.* **2010**, *1*, 411–414.

11 Dogutan, D. K.; McGuire, R., Jr.; Shao-Horn, Y.; Nocera, D. G. Electocatalytic Water Oxidation by Cobalt(III) Hangman β-Octafluoro Corroles. *J. Am. Chem. Soc.* **2011**, *133*, 9178–9180.

12 Sakamoto, W. Protein Degradation Machineries in Plastids. *Annu. Rev. Plant Biol.* **2006**, *57*, 599–621.

13 Aro, E. M.; Virgin, I.; Andersson, B. Photoinhibition of Photosystem II — Inactivation, Protein Damage and Turnover. *Biochim. Biophys. Acta* **1993**, *1143*, 113–134.

14 Andersson, B.; Aro, E. M. Photodamage and D1 Protein Turnover in Photosystem II. In *Regulation of Photosynthesis*; Aro, E. M., Anderson, B., Eds; Kluwer Academic: Dordrecht, The Netherlands, 2001; pp 377—393.

15 Barber, J.; Andersson, B. Too Much of a Good Thing: Light Can Be Bad for Photosynthesis. *Trends Biochem. Sci.* **1992**, *17*, 61–66.

16 Grimes, C. A.; Varghese, O. K.; Ranjan, S. *Light, Water, Hydrogen: The Solar Generation of Hydrogen by Water Photoelectrolysis*; Springer: New York, 2008.

17 Kanan, M. W.; Nocera, D. G. In Situ Formation of an Oxygen-Evolving Catalyst in Neutral Water Containing Phosphate and Co^{2+}. *Science* **2008**, *321*, 1072–1075.

18 Dincă, M.; Surendranath, Y.; Nocera, D. G. A Nickel-Borate Oxygen Evolving Catalyst that Functions under Benign Conditions. *Proc. Natl. Acad. Sci. U.S.A.* **2010**, *107*, 10337–10341.

19 Surendranath, Y.; Dincă, M.; Nocera, D. G. Electrolyte-Dependent Electrosynthesis and Activity of Cobalt Based Water Oxidation Catalysts. *J. Am. Chem. Soc.* **2009**, *131*, 2615–2620.

20 Young, E. R.; Nocera, D. G.; Bulović, V. Direct Formation of a Water Oxidation Catalyst from Cobalt Thin-Films. *Energy Environ. Sci.* **2010**, *3*, 1726–1728.

21 Zhong, D. K.; Sun, J.; Inumaru, H.; Gamelin, D. R. Solar Water Oxidation by Composite Catalyst/alpha-Fe₂O₃ Photoanodes. *J. Am. Chem. Soc.* **2009**, *131*, 6086–6087.

22 Zhong, D. K.; Gamelin, D. R. Photoelectrochemical Water Oxidation by Cobalt Catalyst (Co-Pi)/alpha-Fe₂O₃ Composite Photoanodes: Oxygen Evolution and Resolution of a Kinetic Bottleneck. *J. Am. Chem. Soc.* **2010**, *132*, 4202–4207.

23 Sun, J. W.; Zhong, D. K.; Gamelin, D. R. Composite Photoanodes for Photoelectrochemical Solar Water Splitting. *Energy Environ. Sci.* **2010**, *3*, 1252–1261.

24 Zhong, D. K.; Cornuz, M.; Sivula, K.; Grätzel, M.; Gamelin, D. R. Photo-Assisted Electrodeposition of Cobalt-Phosphate (Co-Pi) Catalyst on Hematite Photoanodes for Solar Water Oxidation. *Energy Environ. Sci.* **2011**, *4*, 1759–1764.

25 Steinmiller, E. M. P.; Choi, K. S. Photochemical Deposition of Cobalt-Based Oxygen Evolving Catalyst on a Semiconductor Photoanode for Solar Oxygen Production. *Proc. Natl. Acad. Sci. U.S.A.* **2009**, *106*, 20633–20636.

26 Seabold, J. A.; Choi, K. S. Effect of a Cobalt-Based Oxygen Evolution Catalyst on the Stability and the Selectivity of Photo-Oxidation Reactions of a WO₃ Photoanode. *Chem. Mater.* **2011**, *23*, 1105–1112.

27 Kanan, M. W.; Yano, J.; Surendranath, Y.; Dincă, M.; Yachandra, V. K.; Nocera, D. G. Structure and Valency of a Cobalt—Phosphate Water Oxidation Catalyst Determined by in situ X-ray Spectroscopy. *J. Am. Chem. Soc.* **2010**, *132*, 13692–13701.

28 Risch, M.; Khare, V.; Zaharieva, I.; Gerencser, L.; Chernev, P.; Dau, H. Cobalt-Oxo Core of a Water-Oxidizing Catalyst Film. *J. Am. Chem. Soc.* **2009**, *131*, 6936–6937.

29 Takahashi, Y.; Gotoh, Y.; Akimoto, J. Single-Crystal Growth, Crystal and Electronic Structure of NaCoO₂. *J. Solid State Chem.* **2003**, *172*, 22–26.

30 Lutterman, D. A.; Surendranath, Y.; Nocera, D. G. A Self-Healing Oxygen-Evolving Catalyst. *J. Am. Chem. Soc.* **2009**, *131*, 3838–3839.

31 Esswein, A. S.; Surendranath, Y.; Reece, S. Y.; Nocera, D. G. Highly Active Cobalt Phosphate and Borate Based Oxygen Evolving Anodes Operating in Neutral and Natural Waters. *Energy Environ. Sci.* **2010**, *4*, 499–504.

32 McAlpin, J. G.; Surendranath, Y.; Dincă, M.; Stitch, T. A.; Stoian, S.; Casey, W. H.; Nocera, D. G.; Britt, R. D. EPR Evidence for Co(IV) Species Produced during Water Oxidation at Neutral pH. *J. Am. Chem. Soc.* **2010**, *132*, 6882–6883.

33 McAlpin, J. G.; Stich, T. A.; Ohlin, C. A.; Surendranath, Y.; Nocera, D. G.; Casey, W. H.; Britt, R. D. Electronic Structure Description of a [Co(III)₃Co(IV)O₄] Cluster: A Model for the Paramagnetic Intermediate in Cobalt-Catalyzed Water Oxidation. *J. Am. Chem. Soc.* **2011**, *133*, 15444–15452.

34 Dimitrou, K.; Folting, W. E.; Streib; Christou, G. Dimerization of the [Co₂ᴵᴵᴵ(OH)₂] Core to the First Example of a [Co₄ᴵᴵO₄] Cubane: Potential Insights into Photosynthetic Water Oxidation. *J. Am. Chem. Soc.* **1993**, *115*, 6432–6433.

35 Symes, M. D.; Surendranath, Y.; Lutterman, D. A.; Nocera, D. G. Bidirectional and Unidirectional PCET in a Molecular Model of a Cobalt—Based Oxygen Evolving Catalyst. *J. Am. Chem. Soc.* **2011**, *133*, 5174–5177.

36 Surendranath, Y.; Kanan, M. W.; Nocera, D. G. Mechanistic Studies of the Oxygen Evolution Reaction by a Cobalt-Phosphate Catalyst at Neutral pH. *J. Am. Chem. Soc.* **2010**, *132*, 16501–16509.

37 Reece, S. Y.; Nocera, D. G. Direct Tyrosine Oxidation using the MLCT Excited States of Rhenium Polypyridyl Complexes. *J. Am. Chem. Soc.* **2005**, *127*, 9448–9458.

38 Irebo, T.; Reece, S. Y.; Sjödin, M.; Nocera, D. G.; Hammarström, L. Proton-Coupled Electron Transfer of Tyrosine Oxidation: Buffer Dependence and Parallel Mechanisms. *J. Am. Chem. Soc.* **2007**, *129*, 15462–15464.

39 Casey, W. H. On the Relative Dissolution Rates of Some Oxide and Orthosilicate Minerals. *J. Colloid Interface Sci.* **1991**, *146*, 586–589.

40 Kirk, D. W.; Ledas, A. E. Precipitate Formation during Sea-Water Electrolysis. *Int. J. Hydrogen Energy* **1982**, *7*, 925–932.

41 Bennett, J. E. Electrodes for Generation of Hydrogen and Oxygen from Seawater. *Int. J. Hydrogen Energy* **1980**, *5*, 401–408.

42 Reece, S. Y.; Hamel, J. A.; Sung, K.; Jarvi, T. D.; Esswein, A. J.; Pijpers, J. J. H.; Nocera, D. G. Wireless Solar Water Splitting Using Silicon-Based Semiconductors and Earth-Abundant Catalysts. *Science* **2011**, *334*, 645–648.

43 Stachurski, J. Z. O.; Pouli, D.; Ripa, J. A.; Pokrzyk, G. F. Low Overvoltage Hydrogen Cathodes. U.S. Patent 4,354,915, Oct 19, 1982.

44 Conway, B. E.; Bai, L. H_2 Evolution Kinetics at High-Activity Ni-Mo-Cd Electrocoated Cathodes and its Relation to Potential Dependence of Sorption of H. *Int. J. Hydrogen Energy* **1986**, *11*, 533–540.

45 Pijpers, J. J. H.; Winkler, M. T.; Surendranath, Y.; Buonassisi, T.; Nocera, D. G. Light-Induced Water Oxidation at Silicon Electrodes Functionalized with a Cobalt Oxygen Evolving Catalyst. *Proc. Natl. Acad. Sci. U.S.A.* **2011**, *108*, 10056–10061.

46 Narasimha, S.; Rohatgi, A.; Weeber, A. W. An Optimized Rapid Aluminum Back Surface Field Technique for Silicon Solar Cells. *IEEE Trans. Electron Devices* **1999**, *46*, 1363–1370.

47 Young, E. R.; Costi, R.; Nocera, D. G.; Bulović, V. Photo-Assisted Water Oxidation with Cobalt-Based Catalyst Formed from Thin-Film Cobalt Metal on Silicon Photoanodes. *Energy Environ. Sci.* **2011**, *4*, 2058–2061.

48 Khaselev, O.; Bansal, A.; Turner, J. A. High-Efficiency Integrated Multijunction Photovoltaic/Electrolysis Systems for Hydrogen Production. *Int. J. Hydrogen Energy* **2001**, *26*, 127–132.

49 Rocheleau, R. E.; Miller, E. L.; Misra, A. High-Efficiency Photoelectrochemical Hydrogen Production using Multijunction Amorphous Silicon Photoelectrodes. *Energy Fuels* **1998**, *12*, 3–10.

50 Kelly, N. A.; Gibson, T. L. Design and Characterization of a Robust Photoelectrochemical Device to Generate Hydrogen using Solar Water Splitting. *Int. J. Hydrogen Energy* **2006**, *31*, 1658–1673.

51 Khaselev, O.; Turner, J. A. A Monolithic Photovoltaic-Photoelectrochemical Device for Hydrogen Production via Water Splitting. *Science* **1998**, *280*, 425–427.

52 Lin, G. H.; Kapur, M.; Kainthla, R. C.; Bockris, J. O'M. One-Step Method to Produce Hydrogen by a Triple Stack Amorphous-Silicon Solar-Cell. *Appl. Phys. Lett.* **1989**, *55*, 386–387.

53 James, B. D.; Baum, G. N.; Perez, J.; Baum, K. N. U.S. DOE, Dec. 2009. Available online at: http://www1.eere.energy.gov/hydrogenandfuelcells/pdfs/pec_techno-economic_analysis.pdf.

54 Nocera, D. G. Chemistry of Personalized Solar Energy. *Inorg. Chem.* **2009**, *48*, 10001–10007.

55 Nocera, D. G. Fast Food Energy. *Energy Environ. Sci.* **2010**, *3*, 993–995.

56 Lewis, N. S.; Nocera, D. G. Powering the Planet: Chemical Challenges in Solar Energy Utilization. *Proc. Natl. Acad. Sci. U.S.A.* **2006**, *103*, 15729–15735.

57 Nocera, D. G. On the Future of Global Energy. *Daedalus* **2006**, *135*, 112–115.